Catalysis Science & Technology

Accepted Manuscript

ROYAL SOCIETY OF CHEMISTRY

www.rsc.org/catalysis

Journal Name

ARTICLE

Silica-immobilized Aquivion PFSA superacid: application to heterogeneous direct etherification of glycerol with *n*-butanol†

Received 00th January 20xx,
Accepted 00th January 20xx

DOI: 10.1039/x0xx00000x

www.rsc.org/

Wenhao Fang,[a,*] Sheng Wang,[b] Armin Liebens,[a] Floryan De Campo,[a] Hualong Xu,[b] Wei Shen,[b] Marc Pera-Titus[a] and Jean-Marc Clacens[a,*]

We report the effective heterogenization of the polymeric perfluorosulfonic acid (PFSA) Aquivion® resin in silica network for the direct etherification of glycerol with aliphatic *n*-butanol. The Aquivion-silica composites, prepared by a template-free sol-gel method, presented a large specific surface area, affording highly accessible acid sulfonic groups. The textural and bulk/surface properties of the hybrid composites were characterized in depth using TGA, acid-base titration, N_2 adsorption-desorption, XRD, TEM, FTIR, Raman, CP-MAS NMR and XPS. The Aquivion-silica composite exhibited a high catalytic activity (91% *n*-butanol conversion) and selectivity (45% butyl glyceryl monoether yield) while it lowered the formation of by-product (6% dibutyl ether yield) as compared to the benchmark homogeneous and heterogeneous acid catalysts. The catalyst was reusable and maintained a stable performance after six consecutive cycles.

1. Introduction

Glycerol, which can be readily obtained as a by-product of biodiesel production processes, is a very attractive renewable raw material.[1-3] Therefore, the conversion of glycerol into valuable chemicals is currently receiving much attention. Many efforts have been made to develop catalytic processes for the transformation of glycerol into valuable chemicals, including dehydration, oxidation, hydrogenolysis, esterification, acetalization, etc.[4-9] Among these different alternatives, the catalytic etherification of glycerol appears to be a promising option that affords the preparation of glyceryl ethers. Glyceryl ethers represent a class of high-value-added chemicals with a huge market. As a matter of fact, it has been shown that glyceryl monoethers from aliphatic alcohols (C_4–C_{12} alcohols) can be used as substitutes for petro-based surfactants in the formulation detergents, personal care products and paints.[10-13] Furthermore, glyceryl polyethers, most specifically di- and tri-butyl (poly-)glyceryl ethers, are often reported as excellent oxygenate additives for bio-diesel reformulation, which could improve the properties of diesel fuels at low temperature and reducing NO_X emission.[14-15]

Most often, butyl glyceryl ethers are produced from the addition of glycerol to isobutene or from the direct etherification of glycerol with *t*-butanol in the presence of acid catalysts. These routes offer a high substrate conversion and high selectivity towards *t*-butyl glyceryl polyethers.[16-19] In contrast, the direct acid-catalyzed etherification of glycerol with aliphatic alcohols such as *n*-butanol is more challenging due to their low selectivity. Indeed, this reaction suffers from the side dehydration and self-etherification of glycerol and alkyl alcohols, as well as from the polyetherification of glycerol and the formation of complex derivatives of glycerol.[12, 20] Conventional catalysts for performing the direct etherification of glycerol with isobutene include mainly acidic homogeneous catalysts and solid acid catalysts such as acidic resins, zeolites and acid-functionalized silica and/or carbon catalysts.[19] However, most of these catalysts can be hardly extrapolated to the direct etherification of glycerol with *n*-butanol. To our knowledge, only two examples have been reported to date showing the optimal selectivity for this reaction. On one hand, some of us reported the benefits of metal triflates,[12] in particular bismuth triflate ($Bi(OTf)_3$), as Lewis catalysts for boosting the selectivity. Nonetheless, sharing the common limitation of homogeneous catalysts, metal triflates cannot be recycled. On the other hand, very recently, Nandiwale *et al.* reported H-beta zeolite as a reusable solid acid for the selective production of glyceryl monoether from *n*-butanol,[20] but the catalyst demonstrated a modest activity. Therefore, the studied reaction presents a major scientific challenge, and successful solutions will imply a smart design of the catalysts and a deeper understanding on the catalytic mechanisms.

During the last two decades, some outstanding developments have been reported in the design of acid-functionalized mesoporous silica as alternatives to commercially available sulfonated polymers, *e.g.* perfluorinated sulfonic acidic resins (PFSA).[21-22] Harmer and co-workers at DuPont were among the

[a] *Eco-Efficient Products and Processes Laboratory (E2P2L), UMI 3464 CNRS/Solvay, 3966 Jin Du Road, Xin Zhuang Ind. Zone, 201108 Shanghai, China. Emails: wenhao.fang@solvay.com; jeanmarc.clacens-ext@solvay.com.*
[b] *Department of Chemistry, Shanghai Key Laboratory for Molecular Catalysis and Innovative Materials and Laboratory of Advanced Materials, Fudan University, 200433 Shanghai, China.*

† Electronic Supplementary Information (ESI) available: textural properties, TGA/DTG profiles, XRD patterns, FTIR spectra, O1s XPS spectra, structures and abbreviations of reactants and possible products. See DOI: 10.1039/x0xx00000x

first authors to develop an efficient sol-gel route for the synthesis of Nafion® resin particles entrapped within a mesoporous silica network *via* alkaline hydrolysis of tetraethyl orthosilicate (TEOS) followed by acidic ion exchange.[23-24] These catalysts showed a high catalytic performance and robustness in a broad spectrum of acid-catalyzed reactions, such as alkylation,[23, 25] olefin isomerization,[24-25] acylation,[26] dimerization,[25, 27] esterification,[28] Friedel-Crafts benzylation,[29] the Fries rearrangement,[30] and the Pechmann reaction.[31] Analogues to these materials based on PFSA-silica composites have been reported.[32-33] Finally, Corma,[34-35] Kaliaguine and Shen[36-38] also designed hybrid materials based on PFSA grafted on MCM-41, SBA-15, and mesocellular silica foams.

Aquivion® PFSA (Scheme 1) is a copolymer based on tetrafluoroethylene and the sulfonyl fluoride vinyl ether produced by Solvay Specialty Polymers. Aquivion represents a new family of perfluorosulfonic superacid resins with an acid strength (Hammett acidity ≈ 12) comparable to that of pure sulfuric acid[23] and a higher thermal stability than Nafion. Aquivion has been explored for applications as proton conductor in PEM fuel cells. However, to the best of our knowledge, no open literature is available to date on the application of Aquivion as acid catalyst. This study is intended to open a window for the potentials of this new acidic resin in catalysis as an extension of its current application scope. However, the recycling of high-acid loading Aquivion PFSA remains great challenging because of its prominent swelling ability in solvents. Moreover, in the form of a coarse powder, Aquivion has a very low surface area (< 0.1 m^2 g^{-1}), whereas the acidity reaches 1.5 mmol g^{-1}. Hence, most of the sulfonic acid sites are expected to be buried within the polymer, leading to a poor accessibility of the reactants to the acid sites. In order to avoid this shortcoming, it would be desirable to develop heterogenized Aquivion catalysts to enhance the contact between the reactants and the active sites.

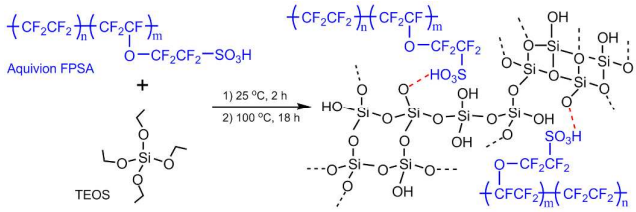

Scheme 1 Possible synthetic route of Aquivion-silica (AqSi-1) composite material.

Herein, we report for the first time an experimental result to prepare silica-immobilized Aquivion PFSA as heterogeneous catalyst for the acid-catalyzed direct etherification of glycerol with *n*-butanol. The synthetic protocol as proposed in Scheme 1 was performed using an improved template-free sol-gel method in the absence of hydrochloric acid, where the sulfonic groups of Aquivion resin realized the acidic hydrolysis and simultaneous polycondensation of silica precursors. This allowed organosulfonic acid groups to be fixed to silica network *via* the formation of covalent bonds and/or electrostatic interactions.[39-40] It was shown that aminosilicates such as 3-aminopropyl trimethoxysilane and 3-aminopropyl triethoxysilicate helped the immobilization of polystyrene sulfonic acid on silica during sol-gel synthesis due to the formation of electrostatic interactions between SO_3H and amino groups.[41-42] In the light of these reports, in complement to TEOS, we evaluated the role of aminosilicate (*i.e.* 3-aminopropyl triethoxysilicate, APTES) as silica precursor, which besides the above mentioned properties lead to generation of environmentally friendly ethanol during hydrolysis, avoiding the presence of methanol in the medium. A series of etherification tests were conducted to assess the effect of the operational variables on the catalytic performance and to evaluate the catalyst stability and reuse.

2. Results and discussion

2.1 Materials characterizations

TGA analyses. Fig. 1 plots the thermal behavior of Aquivion-silica composite materials prepared in this study. For comparison, the thermal profiles of Aquivion PW66-S resin and the bare silica sample are also displayed. Aquivion resin shows a significant weight loss from 280 to 550 °C, which is attributed mainly to the decomposition of the resin. The first zone (280–360 °C) can be associated with a desulfonation process, while the second (360–450 °C) and third zones (450–550 °C) can be related to the decomposition of the side chains and perfluorocarbon backbone,[43] respectively.

The different Aquivion-silica composites show a major weight loss between 400 and 500 °C, which reflects a higher stability of Aquivion after the immobilization compared to the bare polymer. The estimated Aquivion loadings for the different composites are about 30 wt.% (Table 1). Compared to the AqSi-1 composite, the slightly higher loadings are obtained for AqSi-2. This suggests that the presence of amino moieties might probably retain a little more sulfonic groups *via* stronger interactions.[39]

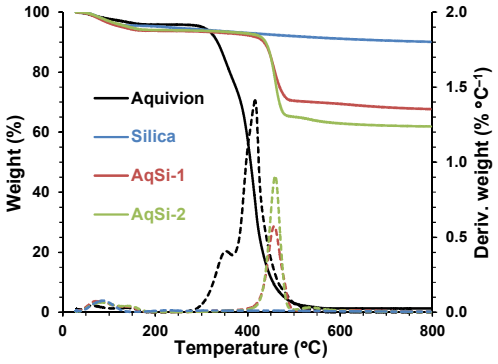

Fig. 1 TGA/DTG profiles of Aquivion, silica and Aquivion-silica composites.

Table 1 Acidic and textural properties of Aquivion, silica and Aquivion-silica composites.

Sample	Aquivion loading (wt.%)	Acidity (mmol g^{-1})[a]	Acidity (mmol g^{-1})[b]	S_{BET} (m^2 g^{-1})	$S_{External}$ (m^2 g^{-1})	V_P (cm^3 g^{-1})	D_P (nm)
Aquivion PW66-S	–	–	1.50	< 0.1	–	–	–
AqSi-1	25	0.38	0.36	358	243	0.16	2.7
AqSi-2	28	0.42	0.40	296	178	0.11	2.6
Silica	–	–	–	714	502	0.28	2.4

[a] Estimated from TGA analyses. [b] Determined by acid-base titration.

After calcination under air, the immobilized Aquivion resin is removed from the composite materials. The calcined samples show a small weight loss (*ca.* 5 wt.%, Fig. S1†) upon heating from room temperature up to 800 °C, matching with the trend observed for the bare silica sample (*ca.* 9 wt.%). The weight loss is mostly due to residual moisture (< 250 °C) and condensation of surface silanol groups (Si–OH) into siloxane bonds (Si–O–Si) at higher temperatures.

Acid-base titration. The acidity of the composite materials as determined by the titration technique is 0.36 mmol g^{-1} for the AqSi-1 catalyst and 0.40 mmol g^{-1} for the AqSi-2 catalyst (Table 1), respectively. These values are consistent with the acidity values that can be deduced from the Aquivion loading by using the acidity of Aquivion PW66-S as a reference (1.5 mmol g^{-1}), which shows a value around 0.40 mmol g^{-1}. Since the bare silica sample exhibits no measurable acidity, the acidities of the different composites must be attributed to highly accessible SO_3H groups belonging to the entrapped Aquivion resin.

N_2 adsorption-desorption isotherms. Fig. 2a reports the N_2 adsorption-desorption isotherms at 77 K on the different Aquivion-silica composites, as well as the bare silica. All the analyzed materials exhibit a type IV isotherm pattern with visible capillary condensation steps. The hysteresis loop observed at a relative pressure (P/P_0) between 0.4 and 0.6 suggests the presence of mesoporous structure. The AqSi-1 composite displays a surface area of about 360 m^2 g^{-1}, while the AqSi-2 composite exhibits a lower value of about 300 m^2 g^{-1}. In addition, AqSi-1 displays the higher external surface area, pore volume and mean pore size (Table 1). Meanwhile, the BET surface, pore volume and mean pore size measured for the bare silica sample show values of 714 m^2 g^{-1}, 0.28 cm^3 g^{-1} and 2.5 nm, respectively. Interestingly, the adsorption and desorption branches in Aquivion-silica composites do not close at low relative pressures, which is a distinct feature of silica-grafted polymer materials.[44-45] The presence of a low-pressure hysteresis loop in the N_2 adsorption-desorption isotherms is often associated to the swelling of an inelastic and non-rigid porous structure during the adsorption cycle,[46] which is related here to the lack of rigidity due to the presence of Aquivion resin inside the pores. Therefore, the comparatively lower surface areas and pore volumes measured on the different Aquivion-silica composites are probably due to a partial pore occupation by the polymer. Besides, different condensation behaviors can exist by using different silicates as precursors, leading to a different distribution of Aquivion resin inside the pores.

After calcination (Fig. 2b), both the specific surface and pore volume of the AqSi-1C sample show a dramatic increase to values of 1044 m^2 g^{-1} and 0.83 cm^3 g^{-1}, respectively (Table S1†). In the case of AqSi-2C sample, the specific surface only shows a moderate decrease, whereas the pore volume evolves to 0.32 cm^3 g^{-1}. The mean pore volumes display an expansion to more than 3 nm for both samples. This evolution of the textural properties reflects the different morphologies of Aquivion-silica composites when using the different silicate precursors. During the sol-gel process, TEOS can self-assemble in the presence of Aquivion resin. In such a case, Aquivion is expected to cover mainly silica nanoparticles and retain in the final pores. Aquivion is regarded to play a role as template, leading to the highly mesoporous AqSi-1C sample (after calcination) with dramatic increase in the surface area when Aquivion is almost removed. If aminosilicate is added to TEOS, this will certainly influence the assembly of silicates, leading in our case to a more compact structure.

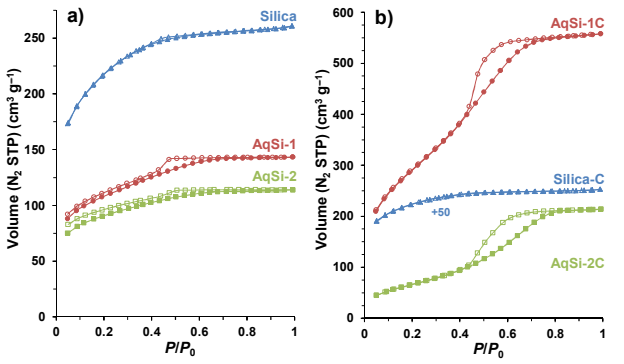

Fig. 2 N_2 adsorption-desorption isotherms at 77 K obtained on a) fresh and b) calcined silica and different Aquivion-silica composites.

XRD analyses. The XRD pattern measured on Aquivion resin displays two broad peaks centered at 16 and 39° that provide a signature of the perfluorocarbon backbone of the amorphous polymer material (Fig. S2a†).[47] In parallel, the bare silica sample shows a characteristic broad peak centered at 23° reflecting its amorphous nature. As expected, different Aquivion-silica catalysts combine the mixed patterns belonging to both the resin and the silica. After calcination, the characteristic peaks corresponding to Aquivion significantly vanish and only the diffraction peak centered at 23° corresponding to silica is preserved (Fig. S2c†).

When inspecting the region of small angles, a distinctive peak at 0.7° can be visualized for the AqSi-1 and AqSi-2 catalysts (Fig. S2b†) and becomes even more visible after calcination, but it cannot be observed for Aquivion resin or the bare silica. Moreover, this peak is preserved and even intensified after calcination (Fig. S2d†). This diffraction peak, which could be certainly better resolved by using Small-Angle X-ray Scattering (SAXS), provides an indication of a characteristic distance for the different composite materials in the range of 10–20 nm that we tentatively associate with the particle size.

TEM measurements. The morphology of the AqSi-1 catalyst, selected here as an illustrative example, was further analyzed by TEM (Fig. 3a). This sample is constituted by very small silica particles with a mean size probably lower than 10–15 nm, which is in agreement with the low-angle XRD pattern and shows an amorphous morphology. In consistent with the N_2 sorption isotherms, the sample shows an assembly of randomly distributed interparticle mesopores. In complement, EDS confirms the presence of fluorine, sulphur and silicon in the sample. When Aquivion is removed by calcination from the composite, the AqSi-1C solid (Fig. 3b) displays also amorphous morphology and even higher proportion of mesopores, showing that Aquivion resin is probably cover mainly silica nanoparticles and retains in the porous structure.

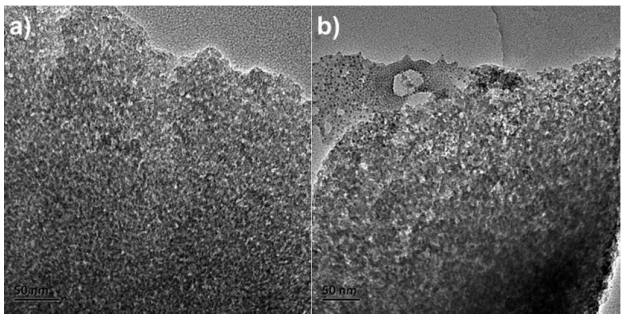

Fig. 3 TEM images of the AqSi-1 and AqSi-1C samples.

FTIR spectra. Fig. 4 reports the FTIR spectra obtained on the different composites, as well as Aquivion resin and the bare silica. Aquivion presents the characteristic bands commonly observed for perfluorosulfonic polymers. The resin shows three bands centered at 1736, 634 and 515 cm^{-1} that can be assigned to CF_2–CF_2 stretching vibration mode. Furthermore, the bands centered at 1154 and 1057 cm^{-1} correspond to SO_3H symmetric stretching mode, while the band 1220 cm^{-1} can be attributed to SO_3H asymmetric stretching mode. Finally, the band appearing at 970 cm^{-1} can be ascribed to C–O–C symmetric stretching mode associated with the side chain of the resin.[23]

The FTIR spectra of different composite materials maintain the same bands as for the original Aquivion resin, even if they appear attenuated. In addition, some new bands attributed to silica are emerging. In particular, the bands appearing at 1080, 955 and 800 and 634 cm^{-1} can be assigned to Si–O–Si cyclic, Si–OH, and Si–O–Si asymmetric stretching modes.[48] These bands can also be observed for the different composites after calcination (Fig. S3†). These results confirm the hybrid nature of the Aquivion-silica catalysts prepared in this study.

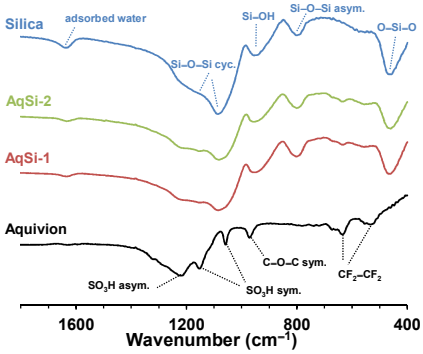

Fig. 4 FTIR spectra of Aquivion, silica and different Aquivion-silica composites.

Raman spectra. Raman spectroscopy, in complement to FTIR, allows further analyzing the vibration modes presented in the composite materials (Fig. 5). Unlike the FTIR spectra, where the Aquivion bands cannot be well distinguished in the different composites due to the presence of the broad and overlapping bands of silica, all the feature bands present in the perfluorosulfonic polymer are well displayed in the composites after immobilization. The most intense band appearing at 735 cm^{-1} can be assigned to CF_2–CF_2 stretching mode coupled to the C–C–C symmetric skeletal stretching of the polymer backbone.[49] The strong bands observed at 393 and 294 cm^{-1} can be associated with CF_2 deformation mode. The symmetric stretching bands belonging to SO_3H and C–S stretching modes are located at 1060 and 800 cm^{-1}, respectively. Noteworthy, the band visible at about 975 cm^{-1} can be regarded as a contribution from both the C–O–C symmetric and Si–O–Si symmetric stretching modes. Additionally, the two bands located at 490 and 610 cm^{-1} correspond to the typical Si–OH asymmetric and Si–O–Si cyclic stretching modes,[48] respectively.

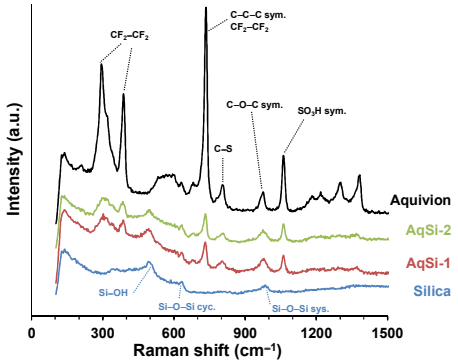

Fig. 5 Raman spectra of Aquivion, silica and different Aquivion-silica composites.

Solid-state NMR measurement. The structural integrity of Aquivion resin and silica framework was further investigated by solid-state NMR (Fig. 6). The AqSi-1 catalyst was selected as the representative sample. The presence of Aquivion domain is evidenced by ^{19}F MAS NMR. The bands of fluorinated polymer are visible mainly at −91, −122 and −151 ppm (strong bands with a characteristic shoulder), which are very similar to the ^{19}F MAS NMR spectrum observed on Nafion resin.[23] These peaks are indicative of fluorine atoms being located within the polymer. The most intense peak at −117 and −122 ppm are originated from fluorine atoms in the polymer backbone. The ^{13}C CP-MAS NMR spectrum shows only one peak centered at 112 ppm, which matches with the chemical shift observed for the Aquivion PFSA resin and reveals that the existence of carbon atoms in the catalyst is mainly due to the polymer.

Finally, the ^{29}Si CP-MAS NMR spectrum shows the typical Q signals centered at −89, −100 and −109 ppm that can be attributed to Q_2, Q_3 and Q_4 silica moieties.[50] The unexpectedly high amount of Q_3 species (*i.e.* Si–OH groups) is consistent with the formation of very small particle sizes, which has been interpreted by the TEM image and the low-angle XRD pattern. Moreover, we cannot rule out a possible restricted motion of silica in water channels of Aquivion, restricting the motion of the silica precursor units during sol-gel synthesis. Such an effect that has been reported for Nafion-silica composites causes a limited condensation of the silica units, which results in a large number of remaining Si–OH groups (Q_3), as well as unreacted $(HO)_2Si(OSi)_2$ moieties (Q_2),[51] in the final composites.

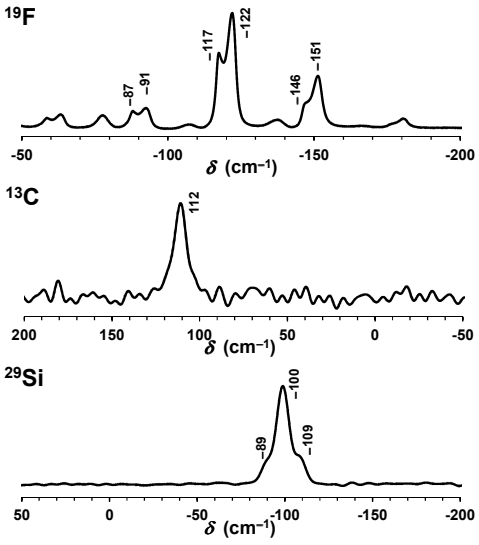

Fig. 6 ^{19}F MAS NMR spectrum, and ^{13}C, ^{29}Si CP-MAS NMR spectra of the AqSi-1 composite.

XPS spectra. The surface compositions of Aquivion-silica hybrid materials was investigated by XPS. As shown in Fig. 7, a single S2p peak can be observed at 168.5 eV for the different composite materials, which is attributed to the presence of SO_3H groups.[52] The F1s peak appears at 687.7 eV, which can be ascribed to fluorine atoms present in the CF_2–CF_2 polymer chains in good agreement with observations on Nafion resin.[52] The C1s peak visible at about 291 eV is assigned to the typical polymer backbone (CF_2–CF_2).[53] Moreover, in the C1s region, three additional peaks appear at 288.4, 285.5 and 284.0 eV, which can be ascribed to the contributions from C–C=O (adventitious carbon species), C–O (side chain) and C–C bonds (symmetric skeletal backbone),[52-53] respectively. Regarding the Si2p spectra, the different composites exhibit a broad peak that can be attributed to the simultaneous presence of Si–OH species (103.4 eV) and Si–O–Si units (102.3 eV)[39, 54] after deconvolution in coherence with the O1s spectra (Fig. S4†). The XPS results confirm the hybrid surface compositions of the Aquivion-silica catalysts.

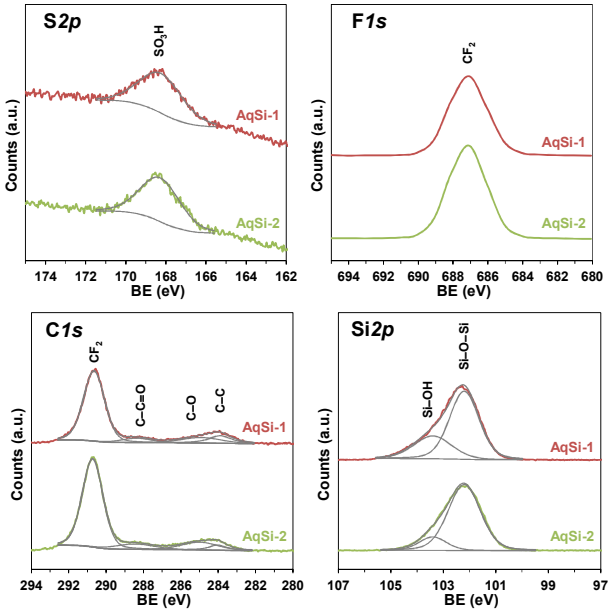

Fig. 7 S2p, F1s, C1s and Si2p XPS spectra of Aquivion and Aquivion-silica composites.

2.2 The etherification of glycerol with *n*-butanol

Effect of reaction time. The etherification of glycerol with *n*-butanol was first studied as a function of the reaction time at 150 °C over the different Aquivion-silica composite catalysts. In all cases, the *n*-butanol conversion and yield to the desired product (B1G1) increase fast during the first 4 h, whereas this trend becomes slower with a longer reaction time (Fig. 8). On the contrary, butyl glyceryl polyethers, including B2G1, B2G2 and B3G2, exhibit slowly linear increase, which is indicative of slower rates of formation. In the case of by-product B2 generated from *n*-butanol dimerization, this reaches a 5% yield just at the beginning of the reaction, and the value stabilizes further at 6%.

In recent kinetic studies on glycerol etherification with *t*-butanol or isobutene,[55-56] three consecutive etherification reactions together with dimerization reaction of *t*-butanol or isobutene were proposed for the reaction mechanism. The product distribution along the reaction confirmed the consecutive transformation from glycerol to mono-, di- and

triglyceryl ethers. In the present study, the different trends of products yield stated above suggest that glycerol etherification with *n*-butanol over the different Aquivion-silica composite catalysts could operate as a tandem process. However, the reaction pathway is far more complicated than that using *t*-butanol or isobutene. In this view (Scheme S1†), glycerol probably reacts first with *n*-butanol to form preferentially B1G1 as the main product, and the dimerization of *n*-butanol or glycerol may be a competitive reaction at this stage. Subsequently, as the reaction progresses, further reaction between the reactants and B1G1 could promote the formation of butyl glyceryl polyethers. To be noted, G2 (diglyceryl ether) probably competes with B1G1 to further react with *n*-butanol. As G2 has more hydroxyl groups than B1G1, G2 is expected to promote the synthesis of highly substituted polyethers matching the decreasing order observed as B3G2 > B2G2 > B2G1. As a matter of fact, some possible products such as monobutyl polyglyceryl ethers, multibutyl polyglyceryl ethers, multibutyl cyclopolyglyceryl ethers were not quantified.

With the different composite materials, the AqSi-1 catalyst shows the better catalytic performance both in terms of *n*-butanol conversion and B1G1 yield (Fig. 8). This observation suggests that a portion of acid sites in the AqSi-2 catalyst might not be accessible to the reactants. More importantly, taking into account that the AqSi-1 catalyst displays the lower acidity, the higher catalytic performance of this sample can be mainly attributed to its higher surface area and pore volume, which would favor a better distribution of acid sites and facilitate the accessibility of the reactants to the acid sites. In the light of these results, we will concentrate our attention in the following studies on the AqSi-1 catalyst for assessing the effect of the reaction conditions on the catalytic properties.

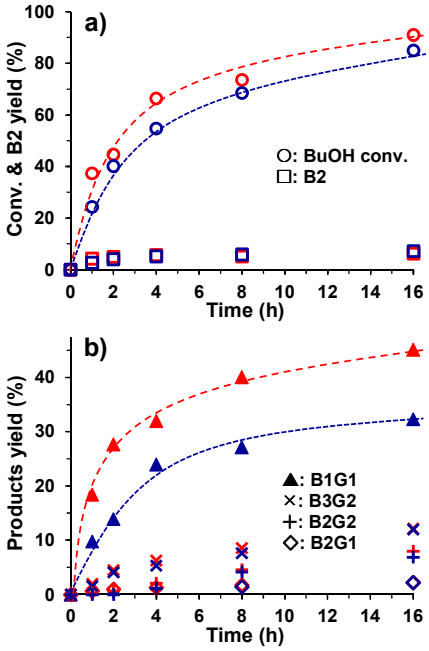

Fig. 8 Conversion of *n*-butanol and yield of products as a function of the reaction time over the AqSi-1 (red) and AqSi-2 (blue) catalysts. Reaction conditions: 5 mmol BuOH, Gly/BuOH molar ratio = 4, 3 mol% H^+ based on BuOH, 150 °C.

Effect of catalyst loading. The influence of the catalyst loading was investigated at 150 °C and at a shorter reaction time (2 h) in order to discourage the formation of glyceryl polyethers (Fig. 9). The catalyst loading is here referred in molar percentage of acidity of the catalyst based on *n*-butanol. The variation of the catalyst loading from 0.9 to 6 mol% H^+ leads to a remarkable increase of the *n*-butanol conversion and B1G1, B2 yields. About 65% *n*-butanol conversion with 36% B1G1 and 11% B2 is obtained over 6 mol% H^+ catalyst. When the catalyst loading is further increased to 9 mol% H^+, a decline in the formation of B1G1 is clearly observed with a concomitant higher formation of B2G2 and B3G2. Moreover, a higher amount of B2 product is also obtained, reaching a yield of about 12%. On the guidance of these results, a catalyst loading at 3 mol% H^+ appears to be a good compromise that can ensure a significant B1G1 yield while discourage the formation of butyl glyceryl polyethers and B2.

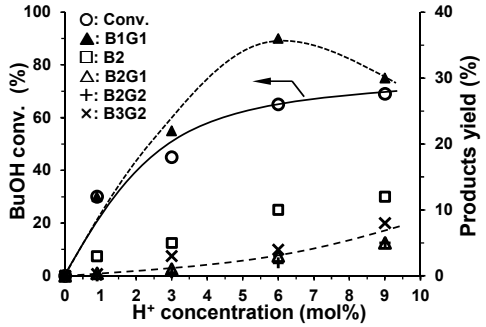

Fig. 9 Conversion of *n*-butanol and yield of products as a function of the catalyst loading over the AqSi-1 catalyst. Reaction conditions: 5 mmol BuOH, Gly/BuOH molar ratio = 4, 150 °C, 2 h.

Effect of reaction temperature. We further investigated the influence of reaction temperature between 120 and 190 °C using a catalyst loading of 3 mol% H^+ (Table 2). No activity is detected at 120 °C after even 24 h of reaction. However, 91% *n*-butanol conversion is obtained at 150 °C after 16 h. An increase of the reaction temperature from 150 to 190 °C has a beneficial effect on the catalytic activity, affording a high *n*-butanol conversion at a shorter reaction time. However, the product distribution depends to an important extent on the reaction temperature. As a matter of fact, the B1G1 yield declines when the temperature increases from 150 to 190 °C in favor of butyl glyceryl polyethers. B1G1 is the main product at 150 °C after 16 h (*ca.* 45%), while butyl glyceryl polyethers (*ca.* 55%) become the main products at 170 °C after 8 h. The B2 yield maintains relatively stable in the temperature range of 150–170 °C, but it clearly increases at 190 °C.

To be remarked it is difficult to compare the selectivity of products as the obtained *n*-butanol conversions are very high (> 90%) between 150 and 190 °C. Besides, reaction time also

varies in each case. Hence, we surveyed, in a further series of tests, the effect of temperature in the range of 150–190 °C but at a very short reaction time for 0.5 h (Table 2). As expected, the *n*-butanol conversion, as well as the yield to the products, increases with the temperature. However, the increase is more pronounced for the different butyl glyceryl polyethers and B2 as compared to B1G1. This observation is consistent with the tendency reported by Nandiwale *et al.* in a recent study which investigated the etherification of glycerol with *n*-butanol over H-beta zeolite. These authors suggested the formation of butylene from the dehydration of *n*-butanol at higher than 160 °C, which might further react with glycerol and/or diglyceryl ether to produce di- and tri-butyl glyceryl ethers.

Table 2 Summary of results for glycerol etherification with *n*-butanol as a function of the reaction temperature over the AqSi-1 catalyst.

Temperature (°C)	Time (h)	Conv. BuOH(%)	Yield B1G1 (%)	Yield B2G1 (%)	Yield B2G2 (%)	Yield B3G2 (%)	Yield B2 (%)
120	24			No reaction			
150	16	91	45	2	8	12	6
170	8	96	22	8	29	18	8
190	3	97	16	9	24	14	16
150	0.5	25	12	1	2	1	4
170	0.5	44	17	3	5	3	6
190	0.5	67	18	6	11	8	13

Reaction conditions: 5 mmol BuOH, Gly/BuOH molar ratio = 4; 3 mol% H^+ based on BuOH.

Catalyst recycling. The recycling of a heterogeneous catalyst is an essential condition for any potential industrial use. To this aim, we carried out a complete recycling study for the AqSi-1 catalyst on a series of etherification tests performed at 150 °C for 16 h. After each test, the catalyst was recovered by high-speed centrifugation, washing in methanol to remove the reactants and products retained by the solid and drying at 120 °C. One should mention that no regeneration of acid sites is needed. The AqSi-1 catalyst shows an optimal stability after six consecutive cycles (Fig. 10), even if a very slight decrease is observed for the *n*-butanol conversion and B1G1 yield (< 5% overall).

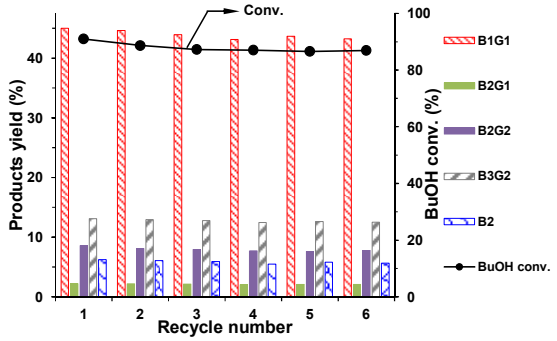

Fig. 10 Recycling tests for the AqSi-1 catalyst for glycerol etherification with *n*-butanol. Reaction conditions: 5 mmol BuOH, Gly/BuOH molar ratio = 4, 3 mol% H^+ based on BuOH, 150 °C, 16 h.

To verify the stability of the AqSi-1 catalyst during the reaction, we further characterized the spent catalyst after reaction. As can be inferred from the TGA analyses (Fig. 11a), the spent catalyst exhibits a very similar weight-loss behavior in nearly the same temperature range compared to the fresh catalyst (24 wt.% *vs.* 25 wt.%), which indicates the lack of significant leaching of SO_3H groups during the reaction. Moreover, the acidity measured by acid-base titration is about 0.34 mmol g^{-1}, which is very close to the value measured on the fresh catalyst (0.36 mmol g^{-1}). This result confirms the lack of leaching of SO_3H groups during consecutive reactions. Moreover, the N_2 isotherm (Fig. 11b), XRD and TEM measurement (not shown here) clearly show the integrity of the mesoporous structure for the spent catalyst despite of a slight decrease of the surface area and pore volume (S_{BET} = 313 m^2 g^{-1}, V_P = 0.10 cm^3 g^{-1}, D_P = 4.1 nm). This observation might be associated with the presence of bulky products inside the catalytic pores after reaction. To verify this hypothesis, the spent catalyst was treated with methanol. The resulting solution analyzed by GC reveals the presence of several product peaks mainly originated from B1G1 and B2 with less butyl glyceryl polyethers. As a matter of fact, it is known that butyl glyceryl polyethers can deactivate sulfonated porous solid acid catalysts due to a partial hindering of acid sites due to their relatively bulky size. In our case, our results reveal that the AqSi-1 catalyst prepared by sol-gel method is a stable solid acid for the present catalytic system with stable porous texture of silica material bearing firmly sulfonic acid sites.

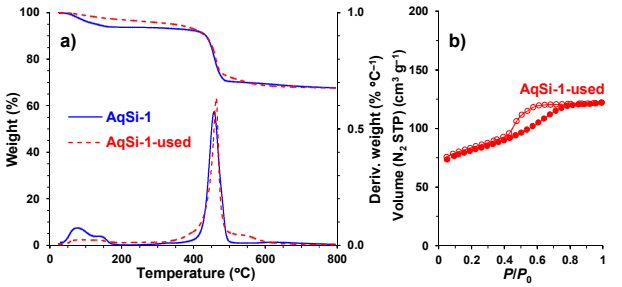

Fig. 11 a) TGA/DTG profiles of the fresh and the used (6 cycles) AqSi-1 catalyst. b) N_2 isotherm of the used (6 cycles) AqSi-1 catalyst.

Comparison with other acid catalysts. Table 3 compares the catalytic performance of the AqSi-1 composite prepared in this study to some typical benchmark acid catalysts. First of all, the

AqSi-1 catalyst is compared with the homogeneous Aquivion PW66-S resin and H_2SO_4 catalyst for the etherification of glycerol with *n*-butanol under the same reaction conditions. Almost the same activity is obtained over the above catalysts, whereas the bare silica demonstrates no activity. Hence, the activity of the AqSi-1 catalyst is related mainly to the Brønsted sulfonic acid sites immobilized by silica. The homogeneous acid catalysts produce less B1G1 but more undesired by-product (B2), probably due to the observed strong intermolecular dehydration reactions.

The comparison of the AqSi-1 catalyst with the well-known heterogeneous sulfonated resins such as Nafion NR50 and Amberlyst-45 reflects a higher activity and yield to etherification products over the former catalyst. Besides, the comparatively better carbon balance seems to also obtain over the AqSi-1 catalyst. We associate these observations not only to the higher acid strength of Aquivion PFSA, but also to the textural and porous properties of the AqSi-1 composite. The enhanced selectivity can be attributed to the higher accessibility to the acid sites and transport effect of reagents, since this catalyst shows much higher surface area, higher pore volume and mesoporosity. These features are expected to lead consequently to a better distribution of acid sites and facilitate their accessibility. In fact, it has been disclosed that sulfonated porous silica materials can boost selectivity of glycerol etherification due to the presence of porous features.[16-17] On the contrary, both Nafion NR50 and Amberlyst-45 exhibit very low surface areas as measured by N_2 adsorption-desorption isotherm at 77 K.

Finally, the AqSi-1 catalyst can be also compared to $Bi(OTf)_3$ that was previously reported by our laboratory as highly selective homogeneous Lewis acid catalyst for glycerol etherification with *n*-butanol.[12] The same conversion can be obtained although $Bi(OTf)_3$ requires necessarily a higher catalyst loading (6.5 mol.% Bi) and a longer reaction time (24 h), resulting in a lower activity. However, $Bi(OTf)_3$ as a Lewis acid offers a comparatively higher yield to B1G1, reaching a value of 70%. The boosted selectivity was probably related to a synergistic effect between $Bi(OTf)_3$ and triflic acid that may be released by glycerolysis of $Bi(OTf)_3$ would enhance the selectivity to B1G1.[12] One must emphasize that the present heterogeneous AqSi-1 catalyst can be easily separated and reused keeping the integrity of the acid sites and porous structure.

Table 3 Catalytic performance of the AqSi-1 catalyst compared to other typical acid catalysts for glycerol etherification with *n*-butanol.

Catalyst	Acidity (mmol g^{-1})	Conv. BuOH (%)	Yield B1G1 (%)	Yield B2G1 (%)	Yield B2G2 (%)	Yield B3G2 (%)	Yield B2 (%)	Activity (mol_{BuOH} mol_{H+})	CB_{BuOH} (%)
AqSi-1	0.36	91	45	2	8	12	6	31	82
Aquivion PW66-S	1.5	89	40	5	4	7	10	30	77
H_2SO_4 [a]	–	88	41	2	3	3	11	29	72
Nafion NR50	0.89	82	29	1	3	5	9	27	65
Amberlyst-45	3.0	76	28	1	4	3	6	25	66
$Bi(OTf)_3$ [a,b]	–	91	70	7	*n.d.*	*n.d.*	10	14	95

Reaction conditions: 5 mmol BuOH, Gly/BuOH molar ratio = 4; 3 mol% H^+ based on BuOH, 150 °C, 16 h. [a] Homogeneous catalyst. [b] Data obtained from previous work[12] under reaction conditions: 10 mmol BuOH, Gly/BuOH molar ratio = 4; 6.5 mol% Bi based on BuOH; 150 °C, 24 h.

3. Experimental

3.1 Materials

A 20 wt.% Aquivion PFSA dispersion in water (D66-20BS ionomer) and its precursor in powder form (PW66-S, equivalent weight: 660 g/equiv, acid loading: 1.5 mmol g^{-1}) were kindly provided by Solvay Specialty Polymers, Italy. Tetraethyl orthosilicate (TEOS, 28 wt.% in silica basis), 3-aminopropyl triethoxysilicate (APTES, 97%), glycerol (99%), *n*-butanol (99.5%), and sulfonic acid (96%) were purchased from Sinopharm Chemical Co., Ltd. Nafion NR50 pellets and Amberlyst-45 pellets (hydrogen form) were purchased from Sigma Aldrich and Dow Chemical, respectively. All the chemicals were used as received without further purification or treatment.

3.2 Preparation of Aquivion-silica composites

Two Aquivion-silica composites were prepared by a sol-gel method using different silicate sources. Typically in a two-necked flask, Aquivion D66-20BS water-dispersion (6.6 g) was added to the given silicate solution, *i.e.* i) TEOS (7.5 g), and ii) APTES (0.2 g)–TEOS (7.5 g). The mixed solution was stirred using a reflux condenser at room temperature for 2 h and further at 100 °C for 18 h. The final solid was centrifuged and washed with excessive deionized water until the supernatant fluid presented a neutral pH. The solid was finally dried at 120 °C for 15 h. The so-prepared catalysts were labeled as AqSi-1 and AqSi-2, respectively. For the sake of comparison, bare silica was also prepared as a reference following the same protocol, but using H_2SO_4 instead of Aquivion as acid source.

To rationalize the structure and morphology of the composite, the samples were calcined at 440 °C under air for 4 h (1 °C min^{-1}) in order to remove Aquivion resin. The calcined solids were labeled with the suffix 'C', *i.e.* AqSi-1C, AqSi-2C, and Silica-C.

3.3 Characterization methods

Thermo gravimetric analysis (TGA/DTG) was carried out on a TA SDT Q600 Instrument. The samples were heated from 30 to 800 °C (10 °C min^{-1}) under air. The heat flow data were dynamically normalized using the instantaneous weight of the sample at the respective temperature.

Acid-base titration was carried out using a Metrohm 794 Basic Titrino system. Prior to the potentiometric titration with NaOH standard solution (0.0101 M calibrated using potassium hydrogen phthalate), the samples (*ca.* 0.1 g) were subjected to ion exchange with a NaCl solution (0.5 M, 50 mL) at room temperature for 24 h.

The textural properties of the samples were measured from N_2 adsorption-desorption isotherms at 77 K on a Micromeritics ASAP 2010 surface area analyzer. The surface areas were calculated by the Brunauer-Emmett-Teller (BET) method from the adsorption branch in the relative pressure range $0.05 < P/P_0 < 0.25$, while the pore volumes were measured at $P/P_0 = 0.99$. The Barrer-Joyner-Halenda (BJH) method was used for measuring intercrystalline mean pore sizes using the adsorption data from the adsorption branch. Prior to the sorption measurements, the samples were degassed at 150 °C for 3 h.

X-ray diffraction (XRD) analysis was performed using a Rigaku D/Max-2200/PC Diffractometer provided with Cu Kα radiation (λ = 1.5418 Å) and a beam voltage of 45 kV. The patterns were registered in the 2ϑ domain (0–70°) with a measured step of 0.02° and a time integration of 0.5 s.

Transition electron microscopy (TEM) measurement was performed on a JEM-2100F field-emission electron microscope operated at an acceleration voltage of 200 kV. Energy dispersive X-ray (EDS) analysis was conducted on an Oxford INCA ENERGY X-Max 20 spectrometer. Samples for TEM measurements were suspended in ethanol and dispersed ultrasonically. Drops of the suspensions were applied on a copper grid coated with carbon.

Fourier transform infrared spectra (FTIR) were recorded on powders dispersed in KBr (2 mg sample in 300 mg KBr) using a Perkin Elmer One FTIR spectrometer with a resolution of 4 cm^{-1} operating in the range of 400–4000 cm^{-1} with 10 scans per spectrum.

Raman spectra were recorded on a Renishaw In Via Raman Microscope spectrometer equipped with a laser beam emitting at 785 nm and a power-output of 15 mW. The spectral resolution was 1 cm^{-1}.

^{13}C and ^{29}Si CP-MAS NMR spectra were recorded on a Bruker AVANCE III 600 WB spectrometer with a 4 mm standard probe spinning at 10 KHz rate. The chemical shifts for ^{13}C and ^{29}Si CP MAS NMR spectra were referenced to the signal of adamantane (δ CH_2 = 38.5 ppm) and 3-(trimethylsilyl)-1-propane-sulfonic acid sodium salt standard (δ = 0.0 ppm), respectively. The ^{19}F MAS NMR spectrum was recorded on a Bruker AVANCE III 400 WB spectrometer with 4 mm standard probe spinning at 11 kHz. Chemical shift of ^{19}F MAS NMR spectrum was referenced to $CFCl_3$.

X-ray photoelectron spectroscopy (XPS) analysis was carried out under ultrahigh vacuum on a Perkin-Elmer PHI 5000C ESCA system provided with Al Kα radiation. The binding energy shift due to the surface charging was adjusted by a reference to the C1s line at 284.5 eV.

3.4 Catalytic test

The etherification reaction was performed on a microwave reaction device. Typically, glycerol (20 mmol), *n*-butanol (5 mmol) and the catalyst (3 mol% H^+ based on *n*-butanol) were well sealed under N_2 in a microwave reactor (6 mL with a pressure limit up to 25 bar) and then continuously stirred (300 r.m.p) at 150 °C for different times. After reaction, the catalytic system was diluted with methanol and the catalyst was recovered by high-speed centrifugation.

The reactants and main products were analyzed using an Agilent 7890 GC equipped with a FID detector and a DB-1 column (10 m length, 0.4 mm inner diameter, 100 am film thickness). The quantification was carried out using the external standard method. Each product as well as *n*-butanol was calibrated with its standard that was diluted in methanol at different concentrations. Scheme S2† compiles the molecular formula of the reactants and all the detected products, as well as their corresponding labels. Minor polyhydroxyl molecules derived from glycerol as well as cyclized by-products, which are very difficult to separate and analyze, were not quantified.[12-13] Carbon balance based on *n*-butanol was accurate within 10% in all the catalytic tests. The conversion of *n*-butanol ($Conv_{BuOH}$), the reaction yield of each product ($Yield_i$) and carbon balance (CB_{BuOH}) were calculated using the following equations.

$$Conv_{BuOH} = \frac{n_{BuOH,initial} - n_{BuOH,final}}{n_{BuOH,initial}} \times 100\%$$

$$Yield_i = \frac{n_i}{n_{BuOH,initial}} \times 100\%$$

$$CB_{BuOH} = \frac{n_{BuOH,final} + \sum n_i}{n_{BuOH,initial}} \times 100\%$$

Conclusions

In the present study, we have shown that the Aquivion® PFSA superacid resin can be effectively immobilized in silica network *via* a one-pot template-free sol-gel method. The Aquivion-silica hybrid composites show a large specific surface area (300–360 $m^2\ g^{-1}$) and a mesoporous structure. The Brønsted acid sites (*ca.* 0.4 mmol g^{-1}) provided by SO_3H groups within Aquivion resin are easily accessible to the reactants. The Aquivion-silica solid acid catalyst (AqSi-1) demonstrates a higher catalytic activity and selectivity in the direct etherification reaction of glycerol with *n*-butanol compared to the typical benchmark homogeneous and heterogeneous acid catalysts, making it a candidate of choice for acid-catalyzed reactions involving biomass-derived reagents. This can be attributed to a combined effect between the strong acid sites of Aquivion resin and the large porosity of silica. The *n*-butanol conversion and yield to butyl glyceryl monoether reached values of 91% and 45%, respectively, at 150 °C with a low catalyst loading of 3 mol% H^+, while the yield to by-product of dibutyl ether was discouraged (6%). The Aquivion-silica catalyst can be reused with no need of regeneration, keeping the integrity of the acid sites and porous structure after 6 catalytic cycles.

Acknowledgements

This work was carried out as a part of collaboration between E2P2L (CNRS/Solvay) and Fudan University. The project was financially supported by CNRS and Solvay. Dr. C. Oldani (Solvay Specialty Polymers, Italy) is warmly acknowledged for providing the Aquivion® PFSA resin and for helpful discussion. The authors would like to express their gratitude to Dr. B. Hu (ECNU) for solid-state NMR measurements, Mr. J. Feng (SICCAS) for TEM measurements and Ms. J. Lu (ANA R&I, Solvay China) for valuable technical assistance.

Notes and references

1. A. Behr, J. Eilting, K. Irawadi, J. Leschinski and F. Lindner, *Green Chem.*, 2008, **10**, 13.
2. Y. Nakagawa and K. Tomishige, *Catal. Sci. Technol.*, 2011, **1**, 179.
3. B. Katryniok, S. Paul and F. Dumeignil, *ACS Catal.*, 2013, **3**, 1819.
4. N. Pethan Rajan, G. S. Rao, V. Pavankumar and K. V. R. Chary, *Catal. Sci. Technol.*, 2014, **4**, 81.
5. B. Katryniok, H. Kimura, E. Skrzynska, J.-S. Girardon, P. Fongarland, M. Capron, R. Ducoulombier, N. Mimura, S. Paul and F. Dumeignil, *Green Chem.*, 2011, **13**, 1960.
6. Z. Xiao, J. Xiu, X. Wang, B. Zhang, C. T. Williams, D. Su and C. Liang, *Catal. Sci. Technol.*, 2013, **3**, 1108.
7. G. Parameswaram, M. Srinivas, B. Hari Babu, P. S. Sai Prasad and N. Lingaiah, *Catal. Sci. Technol.*, 2013, **3**, 3242.
8. C. Gonzalez-Arellano, S. De and R. Luque, *Catal. Sci. Technol.*, 2014, **4**, 4242.
9. M. Hasbi Ab Rahim, Q. He, J. A. Lopez-Sanchez, C. Hammond, N. Dimitratos, M. Sankar, A. F. Carley, C. J. Kiely, D. W. Knight and G. J. Hutchings, *Catal. Sci. Technol.*, 2012, **2**, 1914.
10. P. Gaudin, R. Jacquot, P. Marion, Y. Pouilloux and F. Jérôme, *ChemSusChem*, 2011, **4**, 719.
11. P. Gaudin, R. Jacquot, P. Marion, Y. Pouilloux and F. Jerome, *Catal. Sci. Technol.*, 2011, **1**, 616.
12. F. Liu, K. De Oliveira Vigier, M. Pera-Titus, Y. Pouilloux, J.-M. Clacens, F. Decampo and F. Jerome, *Green Chem.*, 2013, **15**, 901.
13. Z. Fan, Y. Zhao, F. Preda, J.-M. Clacens, H. Shi, L. Wang, X. Feng and F. De Campo, *Green Chem.*, 2015, **17**, 882.
14. T. S. Viinikainen, R. S. Karinen and A. O. I. Krause, in *Catalysis for Renewables*, Wiley-VCH Verlag GmbH & Co. KGaA, 2007, pp. 209.
15. M. J. Climent, A. Corma and S. Iborra, *Green Chem.*, 2014, **16**, 516.
16. M. D. González, Y. Cesteros, J. Llorca and P. Salagre, *J. Catal.*, 2012, **290**, 202.
17. M. D. González, P. Salagre, E. Taboada, J. Llorca, E. Molins and Y. Cesteros, *Appl. Catal. B*, 2013, **136–137**, 287.
18. M. D. Gonzalez, P. Salagre, E. Taboada, J. Llorca and Y. Cesteros, *Green Chem.*, 2013, **15**, 2230.
19. J. Zhou, Y. Wang, X. Guo, J. Mao and S. Zhang, *Green Chem.*, 2014, **16**, 4669.
20. K. Y. Nandiwale, S. E. Patil and V. V. Bokade, *Energy Technology*, 2014, **2**, 446.
21. A. F. Lee and K. Wilson, in *Handbook of Green Chemistry*, Wiley-VCH Verlag GmbH & Co. KGaA, 2010.
22. R. Ciriminna, P. Demma Carà, J. A. Lopez-Sanchez and M. Pagliaro, *ChemCatChem*, 2014, **6**, 3053.
23. M. A. Harmer, W. E. Farneth and Q. Sun, *J. Am. Chem. Soc.*, 1996, **118**, 7708.
24. Q. Sun, M. A. Harmer and W. E. Farneth, *Chem. Commun.*, 1996, 1201.
25. M. A. Harmer, Q. Sun, A. J. Vega, W. E. Farneth, A. Heidekum and W. F. Hoelderich, *Green Chem.*, 2000, **2**, 7.
26. H. Schuster and W. F. Hölderich, *Appl. Catal. A*, 2008, **350**, 1.
27. Q. Sun, W. E. Farneth and M. A. Harmer, *J. Catal.*, 1996, **164**, 62.
28. M. J. Climent, A. Corma, S. Iborra, S. Martínez-Silvestre and A. Velty, *ChemSusChem*, 2013, **6**, 1224.
29. Q. Sun, M. A. Harmer and W. E. Farneth, *Ind. Eng. Chem. Res.*, 1997, **36**, 5541.
30. R. Hinze, M. C. Laufer, W. F. Hölderich, W. Bonrath and T. Netscher, *Catal. Today*, 2009, **140**, 105.
31. M. C. Laufer, H. Hausmann and W. F. Hölderich, *J. Catal.*, 2003, **218**, 315.
32. K. Okuyama, X. Chen, K. Takata, D. Odawara, T. Suzuki, S.-i. Nakata and T. Okuhara, *Appl. Catal. A*, 2000, **190**, 253.
33. M. Fujiwara, K. Shiokawa and Y. Zhu, *J. Mol. Catal. A*, 2007, **264**, 153.
34. M. Alvaro, A. Corma, D. Das, V. Fornes and H. Garcia, *Chem. Commun.*, 2004, 956.
35. M. Alvaro, A. Corma, D. Das, V. Fornés and H. García, *J. Catal.*, 2005, **231**, 48.
36. W. Shen, D. Dubé and S. Kaliaguine, *Catal. Commun.*, 2008, **10**, 291.
37. W. Shen, Y. Gu, H. Xu, D. Dubé and S. Kaliaguine, *Appl. Catal. A*, 2010, **377**, 1.
38. Z. Huang, W. Pan, H. Zhou, F. Qin, H. Xu and W. Shen, *ChemSusChem*, 2013, **6**, 1063.
39. H. Zou, S. Wu and J. Shen, *Chem. Rev.*, 2008, **108**, 3893.
40. X. Zhang, F. Su, D. Song, S. An, B. Lu and Y. Guo, *Appl. Catal. B*, 2015, **163**, 50.
41. R. Tamaki and Y. Chujo, *Chem. Mater.*, 1999, **11**, 1719.
42. I. Sádaba, M. Ojeda, R. Mariscal and M. L. Granados, *Appl. Catal. B*, 2014, **150–151**, 421.
43. Z. Chai, C. Wang, H. Zhang, C. M. Doherty, B. P. Ladewig, A. J. Hill and H. Wang, *Adv. Funct. Mater.*, 2010, **20**, 4394.
44. F. Zhang, Y. Meng, D. Gu, Yan, C. Yu, B. Tu and D. Zhao, *J. Am. Chem. Soc.*, 2005, **127**, 13508.
45. H. Kassab, M. Maksoud, S. Aguado, M. Pera-Titus, B. Albela and L. Bonneviot, *RSC Adv.*, 2012, **2**, 2508.
46. V. K. Shahi, *Solid State Ionics*, 2007, **177**, 3395.
47. J. Chabé, M. Bardet and G. Gébel, *Solid State Ionics*, 2012, **229**, 20.
48. Y. Liang, C. R. Miranda and S. Scandolo, *J. Chem. Phys.*, 2006, **125**.
49. J. Zeng, D.-i. Jean, C. Ji and S. Zou, *Langmuir*, 2011, **28**, 957.

50. J. Wei, X. Zhang, X. Zhang, Y. Zhao, R. Li and Q. Yang, *ChemCatChem*, 2014, **6**, 1368.
51. G. Ye, C. A. Hayden and G. R. Goward, *Macromolecules*, 2007, **40**, 1529.
52. C. Chen, G. Levitin, D. W. Hess and T. F. Fuller, *J. Power Sources*, 2007, **169**, 288.
53. M. V. Martínez de Yuso, L. A. Neves, I. M. Coelhoso, J. G. Crespo, J. Benavente and E. Rodríguez-Castellón, *Fuel Cells*, 2012, **12**, 606.
54. Y. Zhang, X. He, J. Ouyang and H. Yang, *Sci. Rep.*, 2013, **3**.
55. M. P. Pico, A. Romero, S. Rodríguez and A. Santos, *Ind. Eng. Chem. Res.*, 2012, **51**, 9500.
56. J. Liu, B. Yang and C. Yi, *Ind. Eng. Chem. Res.*, 2013, **52**, 3742.

Journal Name

ARTICLE

Table of Contents

Silica-immobilized Aquivion® resin with high mesoporosity and acid-sites accessibility demonstrated good activity, selectivity and reusability for glycerol etherification with *n*-butanol.

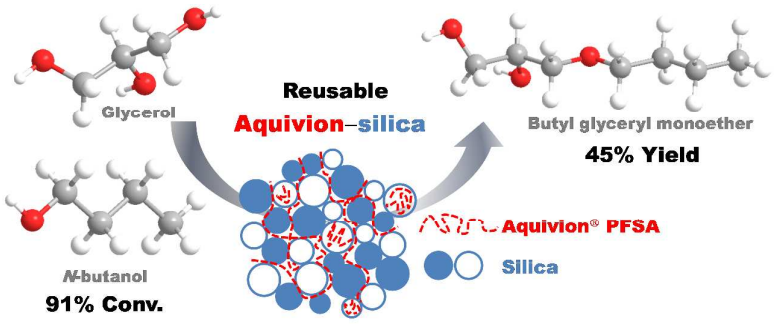

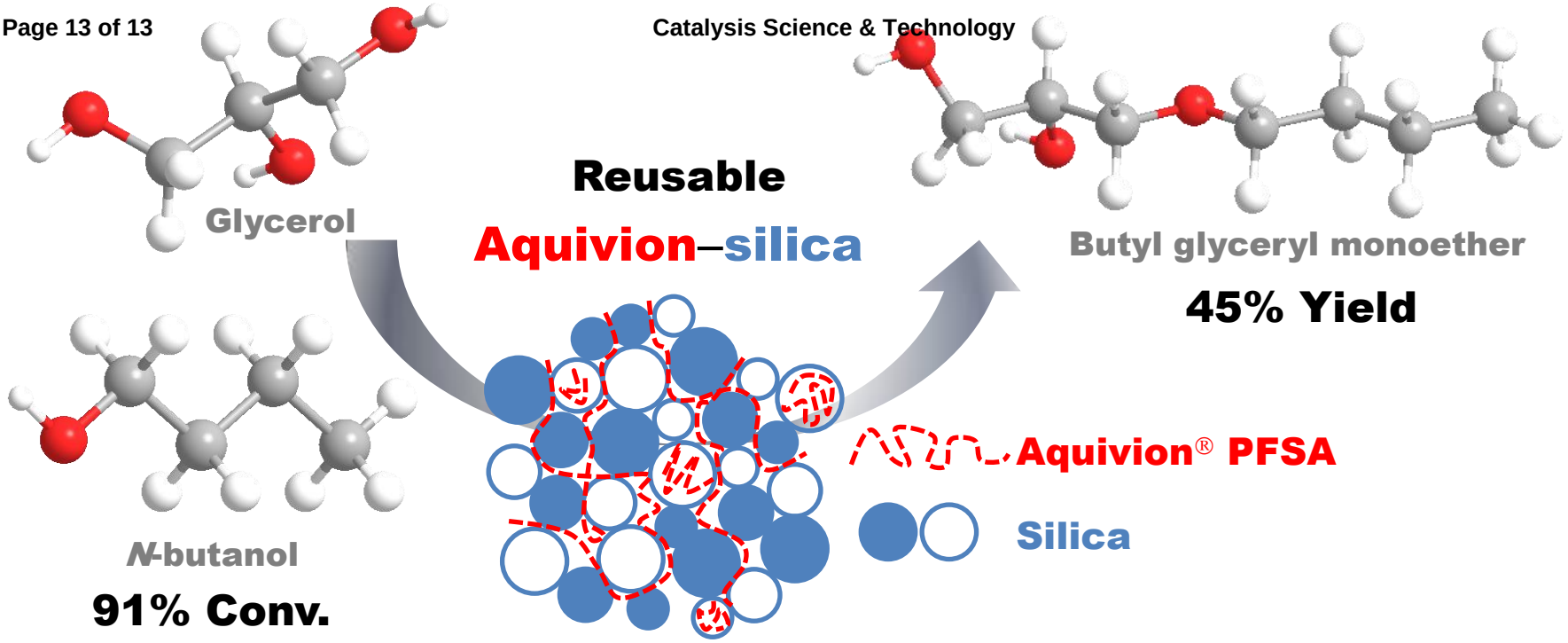

Silica-immobilized Aquivion® resin with high mesoporosity and acid-sites accessibility demonstrated good activity, selectivity and reusability for glycerol etherification with *n*-butanol.